# A Methanol-Tolerant Carbon-Supported Pt−Au Alloy Cathode Catalyst for Direct Methanol Fuel Cells and Its Evaluation by DFT

**G. Selvarani,[†] S. Vinod Selvaganesh,[†] S. Krishnamurthy,[†] G. V. M. Kiruthika,[†] P. Sridhar,[†] S. Pitchumani,[†] and A. K. Shukla*[,†,‡]**

*Central Electrochemical Research Institute, Karaikudi-630006, India, and Solid State and Structural Chemistry Unit, Indian Institute of Science, Bangalore-560012, India*

*Received: December 12, 2008; Revised Manuscript Received: February 14, 2009*

A Pt−Au alloy catalyst of varying compositions is prepared by codeposition of Pt and Au nanoparticles onto a carbon support to evaluate its electrocatalytic activity toward an oxygen reduction reaction (ORR) with methanol tolerance in direct methanol fuel cells. The optimum atomic weight ratio of Pt to Au in the carbon-supported Pt−Au alloy (Pt−Au/C) as established by cell polarization, linear-sweep voltammetry (LSV), and cyclic voltammetry (CV) studies is determined to be 2:1. A direct methanol fuel cell (DMFC) comprising a carbon-supported Pt−Au (2:1) alloy as the cathode catalyst delivers a peak power density of 120 mW/cm$^2$ at 70 °C in contrast to the peak power density value of 80 mW/cm$^2$ delivered by the DMFC with carbon-supported Pt catalyst operating under identical conditions. Density functional theory (DFT) calculations on a small model cluster reflect electron transfer from Pt to Au within the alloy to be responsible for the synergistic promotion of the oxygen-reduction reaction on a Pt−Au electrode.

## 1. Introduction

Among the various fuel cell systems under active development, polymer electrolyte fuel cells (PEFCs) are considered to be most attractive because of their quick start-up and ambient-temperature operation. The main drawback with the hydrogen-fueled PEFCs is the difficulty of generating, handling, and storing hydrogen. In the literature,[1−6] efforts are therefore being expended to directly use hydrogen-bearing organic fuels, such as methanol, ethanol, propanol, formic acid, dimethyl ether, and ethylene glycol, for directly fueling PEFCs. Among these, methanol because of its high specific energy-density and ease to handle happens to be the most attractive fuel.[7−9] PEFCs directly fueled with methanol are referred to as direct methanol fuel cells (DMFCs).

One of the problems limiting the commercialization of DMFCs has been the methanol cross-over across the polymer electrolyte membrane. Methanol cross-over affects the performance of the cathode owing to methanol adsorption on Pt sites in the catalyst, as, under such a situation, the catalyst sites that ought to be performing the reduction of oxygen induce concomitant oxidation of methanol at the cathode resulting in a mixed potential that decreases the cell voltage and hence the performance of the DMFC.[1,2,10−12] The methanol cross-over problem can be mitigated by restricting the methanol permeability of the polymer electrolyte membrane and also by employing a suitable methanol-tolerant cathode catalyst.[13]

In the literature,[14−18] the latter aspect has been studied by addition of base metals, such as cobalt, iron, nickel, and chromium, to platinum metal, but these catalysts are found prone to base-metal dissolution. Owing to this problem, introduction of second noble metal, such as palladium or gold, with platinum has attracted the attention of various researchers and has become a subject of investigation in recent years.[19−22] Among these, gold happens to be the most attractive catalyst because of its inertness in the bulk state and high catalytic activity at nanoscale;[23−26] gold when alloyed with platinum provides enhanced activity toward oxygen reduction reaction (ORR).[27−33] Besides, gold is known to have a stabilizing effect on Pt even under highly oxidizing conditions.[33]

Although Pt−Au nanoparticles supported on silica have been studied extensively,[34] the studies of electrocatalytic oxygen reduction using Pt−Au remain scant in the literature. Only a few studies demonstrating the suitability of Pt−Au nanoparticles for fuel cell application are reported; for example, recently, it has been demonstrated that the preparation route for a bimetallic Pt−Au nanoparticle electrocatalyst influences the ORR in both a DMFC and a PEFC.[19,31−33] But these studies lack a systematic physical characterization of Pt−Au nanocatalysts in conjunction with electrochemistry that are seminal to further our understanding of these catalysts and also the performance of the fuel cells utilizing them.

In general, a bimetallic substance differs in properties from its single metal counterparts, as the presence of another metal atom in the parent lattice affects its composition, crystal structure, and electronic nature. These factors are known to influence the catalytic behavior of a bimetallic alloy and are primarily driven by the experimental conditions used for its preparation. In the present study, a Pt−Au alloy catalyst with varying atomic weight ratios, namely 1:1, 2:1, and 3:1, is supported on carbon. The extent of alloy formation, mean particle size, surface morphology, and oxidation states of individual constituents of Pt−Au/C are determined from powder X-ray diffraction (XRD), transmission electron microscopy (TEM), and X-ray photoelectron spectroscopy (XPS) studies, respectively. The optimum atomic ratio of Pt to Au in the Pt−Au alloy toward ORR in a DMFC is determined by cyclic voltammetry (CV) and linear-sweep voltammetry (LSV) in conjunction with cell polarization.

* To whom correspondence should be addressed. Tel.: +91-4565-227777; fax: +91-4565-227779; e-mail: akshukla2006@gmail.com.
[†] Central Electrochemical Research Institute.
[‡] Indian Institute of Science.

10.1021/jp810970d CCC: $40.75 
Published on Web 04/03/2009

Since the electrocatalytic activity of a material is related to its electronic structure, DFT (density functional theory) calculations have been employed to analyze the electronic structure of Pt−Au alloys and their ameliorating catalytic activity as compared to the bare Pt nanocluster. Recently, in the literature,[34−37] structure and electronic properties of Pt−Au cluster have been studied by DFT. But these studies are limited to subnanometer-sized metal clusters (≤12 atoms) and require extension to bigger clusters to further the understanding of their electronic structure. Accordingly, this study includes DFT calculations on the structure and electronic properties of $Pt_{15}$ $Au_5$ and $Pt_{10}$ $Au_{10}$ alloy clusters in conjunction with $Au_{20}$ and $Pt_{20}$ bare clusters to corroborate our experimental findings.

## 2. Experimental Section

**2.1. Preparation of Carbon-Supported Pt−Au Alloy.** For the preparation of platinum−metal precursor, a chemical route reported elsewhere[38] was adopted. To prepare carbon-supported platinum−gold (Pt−Au/C) nanoparticles, the required amount of hydrogen tetrachloroaurate ($HAuCl_4$) solution was taken and $Na_2[Pt(SO_3)_4]$, dissolved in aq $H_2SO_4$ (0.1 mM), was added to it drop-by-drop at 40 °C followed by addition of 50 mL of hydrogen peroxide (15 w/o) with continuous mechanical stirring at 60 °C accompanied with vigorous gas evolution. The solution was further stirred for 1 h. Subsequently, the required amount of Vulcan XC-72R carbon slurry in water was added to it. Finally, carbon-supported platinum−gold (Pt−Au/C) was obtained by passing hydrogen gas for 2 h at 80 °C, which was filtered, washed copiously with hot distilled water, and dried in an air oven at 80 °C for 2 h. Varying atomic weight ratios of Pt−Au/C alloy catalysts, namely 3:1, 2:1, and 1:1, were prepared similarly keeping the contents of Pt as 40 w/o. Carbon-supported Pt (40 w/o) was also prepared by the aforesaid procedure.

**2.2. Physical Characterization.** Powder XRD patterns for various carbon-supported Pt−Au catalysts were obtained on a Philips X'Pert Diffractometer using Cu Kα radiation ($\lambda$ = 1.5406 Å) between 20° and 80° in reflection geometry in steps of 0.034°/min. The morphology of samples was examined under a TCNAI 20 G2 transmission electron microscope (200 kV). For this purpose, samples were suspended in isopropyl alcohol and cast by dropping the catalyst solution onto a carbon-coated copper grid followed by solvent evaporation in vacuum at room temperature (∼25 °C).

XPS for the Pt−Au/C catalysts were recorded on a MultiLab 2000 (Thermofisher Scientific, UK) X-ray photoelectron spectrometer fitted with a twin anode X-ray source using Mg Kα radiation (1253.6 eV). For recording the desired spectrum, a powder sample was pressed onto a conducting carbon tape pasted onto the indium-coated SS stubs. The sample stubs were initially kept in the preparatory chamber overnight at $10^{-9}$ mbar for desorbing any volatile species and were introduced into the analysis chamber at $9.8 \times 10^{-10}$ mbar for recording the spectra. High-resolution spectra averaged over five scans with a dwell time of 100 ms in steps of 0.02 eV were obtained for all the catalyst samples at the pass energy of 20 eV in constant analyzer energy mode. Experimental data were curve fitted with a Gaussian and Lorentzian mix-product function after subtracting Shirley background. Spin−orbit splitting and the doublet intensities were fixed as described in the literature.[39] Relative intensities of the surface species were estimated from the respective areas of the fitted peaks.

Inductively coupled plasma optical emission spectrometry (ICP-OES) was used to analyze the composition of the as-synthesized Pt/C and Pt−Au/C catalysts. For this purpose, the catalysts were dissolved in concentrated aquaregia followed by dilution with water to concentrations ranging between 1 and 50 ppm as desired for the analysis. The actual composition was determined from the calibration curves of the known standards. The surface morphology for various Pt−Au catalysts were studied using a JEOL JSM 5400 scanning electron microscope (SEM), and their atomic compositions were obtained with the help of the Energy Dispersive X-ray Analysis (EDAX) facility.

**2.3. Electrochemical Characterization.** ***2.3.1. Half-Cell Mode.*** To study the ORR activity and methanol tolerant ability of Pt/C and various Pt−Au/C catalysts, LSV and CV measurements were performed using a computer-controlled electrochemical analyzer (Autolab PGSTAT-30).

A glassy carbon (GC) disk with geometrical area of 0.07 $cm^2$ was used as a working electrode substrate for CV and LSV measurements. Prior to each test, the electrode was polished with 0.06 $\mu$m alumina to obtain a mirror-like finish followed by rinsing with triple-distilled water in an ultrasonic bath. A saturated calomel electrode (SCE) and Pt foil were used as reference and counter electrodes, respectively, in the three-electrode configuration. During the measurements, a gentle flow of nitrogen or oxygen was maintained over the electrolyte surface. All electrochemical experiments were carried out at 25 °C.

To prepare the working electrode, the suspension of the catalyst (Pt/C or Pt−Au/C) was obtained by adding 10 mg of catalyst in 4 mL of water mixed with 30 w/o Nafion solution (DuPont) followed by sonication for 30 min. The suspension was quantitatively transferred to the surface of the polished GC disk. The electrode was dried at room temperature (∼25 °C). In order to clean and activate the electrode surface, a series of CV experiments were conducted in nitrogen-purged blank (aq 0.5 M $H_2SO_4$) electrolyte. The electrode was cycled between −0.25 and 0.8 V with respect to SCE at a sweep rate of 50 mV/s to obtain stable and reproducible voltammograms.

***2.3.2. Fuel Cell Studies.*** *(a) Fabrication of Membrane Electrode Assemblies (MEAs).* MEAs were fabricated adopting the procedure described elsewhere.[39] In brief, both anode and cathode comprise a backing layer, a gas-diffusion layer, and a reaction (catalyst) layer. A teflonized (15 w/o) carbon paper (Toray-TGP-H-120) of 0.35 mm thickness was employed as the backing layer to these electrodes. To prepare the gas-diffusion layer, Vulcan-XC72R carbon was suspended in cyclohexane and agitated in an ultrasonic water bath for 30 min. To this was added 15 w/o Teflon suspension under sonication. The resultant slurry was spread onto a teflonized carbon paper and sintered at 350 °C for 30 min.

To prepare the catalyst layer for DMFCs, the required amount of the catalyst (Pt/C or Pt−Au/C) was suspended in isopropyl alcohol. The mixture was agitated in an ultrasonic water bath and 30 w/o of Nafion (Dupont) solution was added to it with continuous agitation for 1 h. The resulting ink was coated onto the gas-diffusion layer of the electrode. The platinum metal loading at cathode was 2 $mg_{Pt}/cm^2$, which was kept identical for all MEAs. For anodes, 2 $mg_{Pt}/cm^2$ of carbon-supported Pt−Ru (Alfa Aesar) catalyst with 10 w/o Nafion was used.

To establish effective contact between the catalyst layer and the polymer electrolyte, a thin layer of Nafion solution (5 w/o) diluted with isopropyl alcohol in 1:1 ratio was spread onto the surface of each electrode, namely cathode and anode. MEAs were obtained by hot pressing, under 60 kg $cm^{-2}$ at 130 °C for 3 min, the cathode and anode placed on either side of a pretreated Nafion-117 membrane for operating with a DMFC.

*(b) Polarization Studies on DMFCs.* MEAs for DMFCs were evaluated using a conventional 25 $cm^2$ fuel-cell fixture with parallel-serpentine flow-field machined on graphite plates (M/s Schunk Kohlenstofftechnik GmbH, Germany). After equilibration, DMFC single cells were tested at 70 °C with aqueous methanol at a flow rate of 30 mL/min at anode and humidified gaseous oxygen at a flow rate of 0.5 L/min at cathode at atmospheric pressure.

**2.4. Computational Details and Model Clusters.** DFT calculations have been effectively employed for analyzing the electronic properties of transition metals.[40] In the present study, DFT calculations were carried out using VASP (Vienna ab initio Simulation Package) software[41] by considering the valance electrons. The core-valance electron interactions were treated by PAW (Plane Augmented Wave) pseudopotentials.[42,43] In addition, a generalized gradient approximation (GGA) of Perdew−Wang (PW91) was used for all the systems.[44] The plane wave basis set was employed with an energy cutoff at 400 eV. The metallic cluster was placed in a cell with 10 Å distance between the neighboring images. The convergence for the energy cutoff and cell size was found by gradual increments in energy cutoff values and the cell size. Bearing in mind that gold has relativistic effects,[45] scalar relativistic effects were included for all the clusters studied here.

$Au_{20}$ cluster is tetrahedral with its faces resembling the fcc (111) structure on nanoscale.[46] On the basis of the powder X-ray diffraction data discussed in the following section, an $Au_{20}$ atom cluster was preferred with this geometry as the starting point. All the Au atoms in $Au_{20}$ cluster were replaced by the Pt atoms to obtain pure $Pt_{20}$ cluster. $Pt_{10}Au_{10}$ (1:1) and $Pt_{15}Au_5$ (3:1) alloy clusters were obtained by substitution of Au into $Pt_{20}$ cluster. For the alloy composition, Pt atoms in $Pt_{20}$ were replaced by Au atoms to realize $Pt_{10}Au_{10}$ (1:1) and $Pt_{15}Au_5$ (3:1) clusters with Au atoms at varying atomic positions leading to about 20 starting geometries for each composition. These clusters were then optimized to obtain the most stable Au−Pt alloy geometry for each composition. The electronic properties, such as energy gap between the highest occupied molecular orbital (HOMO) and lowest unoccupied molecular orbital (LUMO), atomic charges, and charge density, were analyzed for resultant geometry. Subsequently, the results were compared with homogeneous Pt and Au clusters.

## 3. Results and Discussion

**3.1. Physical Characterization of Catalysts.** XRD patterns for Pt/C and Pt−Au/C are shown in Figure 1. For clarity, the diffraction patterns between 30° and 50° have been enlarged in Figure 1b. The XRD patterns (Figure 1a) for both Pt/C and Pt−Au/C show peaks corresponding to (111), (200), (220), and (311) planes characteristic of a face-centered cubic (fcc) structure. The XRD data also clearly reflects that the Pt−Au/C catalyst forms a solid solution. The XRD peak corresponding to the (111) plane for pure Pt is seen at 39.6° and that for pure gold at 38.2°. The platinum (111) plane for Pt−Au/C catalyst lies at 38.7° and the negative shift in (111) peak position in relation to Pt/C confirms the alloy formation in the Pt−Au catalyst.

A judicious selection of preparatory conditions, in particular, the heating rate and the final reaction temperature, is mandatory for synthesizing finely divided Pt−Au alloy particles.[29] The average size of the Pt−Au alloy nanoparticles is estimated by using the Scherrer equation: $d = 0.94\lambda_{k\alpha 1}/B_{(2\theta)} \cos \theta_B$, where $d$ is the average particle diameter, $\lambda_{k\alpha 1}$ is the wavelength of X-ray radiation (1.5406Å), $\theta_B$ is the Bragg angle for the (111) peak,

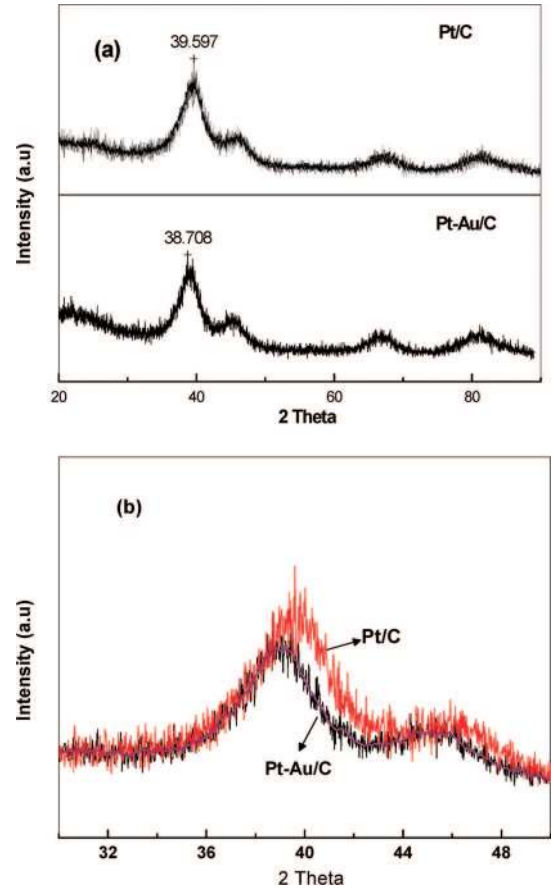


**Figure 1.** (a) Powder X-ray diffraction patterns for Pt/C and (2:1) Pt−Au/C catalysts, (b) X-ray diffraction patterns for Pt/C and Pt−Au/C catalysts between 30° and 50° ($2\theta$).

**TABLE 1: Composition and Structural Parameters for Pt/C and Pt−Au/C Alloy Catalysts with Varying Atomic Ratios**

| catalyst | particle size TEM (nm) | particle size XRD (nm) | atomic ratio (ICP-OES) in % | atomic ratio (EDAX) in % |
|---|---|---|---|---|
| Pt/C | 3.5 | 3.9 | − | − |
| (3:1)Pt−Au/C | 4.3 | 4.6 | 74.35:25.65 | 71.65:28.35 |
| (2:1)Pt−Au/C | 4.5 | 4.9 | 65.8:34.2 | 66.25:33.75 |
| (1:1)Pt−Au/C | − | 5.3 | 49.44:50.55 | 50.31:49.69 |

and $B_{(2\theta)}$ is the full-width at half-maximum (in radians) for the diffraction peak. The average particle sizes for the catalysts thus obtained are presented in Table 1. From the broadening of the (111) diffraction peak and by using the Debye−Scherrer equation, it is seen that the mean particle size for all Pt−Au alloy catalysts is slightly larger in relation to the Pt/C catalyst. Interestingly, the mean particle size increases with increasing Au content in the Pt−Au alloy. Since these catalyst exhibit similar crystal structure, it is convenient to assess their electrocatalytic activity toward ORR.

Figure 2 shows TEM images for the carbon-supported Pt−Au alloy catalyst with varying Pt to Au atomic ratios. As can be seen, the Pt−Au alloy nanoparticles with a narrow particle-size distribution are well dispersed on the surface of the support. In the study, the mean size of the metal nanoparticles on carbon support is obtained by measuring 200 randomly chosen particles in the magnified TEM images (Table 1). For the Pt−Au (3:1) alloy catalyst, the mean particle size has a diameter of about 4.5 nm with a narrower size distribution than for Pt−Au (2:1) and Pt−Au (1:1) catalysts. The mean particle size for the Pt−Au

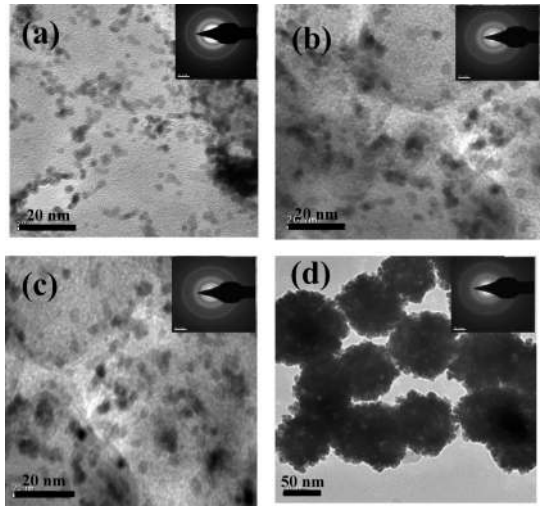


**Figure 2.** Transmission electron microscopy micrograph and electron diffraction patterns for carbon-supported (a) Pt and Pt−Au bimetallic samples with varying Pt to Au atomic ratios, namely (b) 3:1, (c) 2:1, and (d) 1:1.

(2:1) and Pt−Au (1:1) alloy catalysts increases with increasing Au content. These values are in good agreement with the XRD data. Although the XRD data for (1:1) Pt−Au/C show nanometer level particles, the TEM picture for (1:1) Pt−Au/C shows cluster particles. The high metal to support ratio in the samples is likely to induce such aggregation effects.

Electron diffraction patterns for Pt/C and Pt−Au/C with varying atomic ratios of Au and Pt obtained from a selected area in Figure 2 (main figure) are presented in inset of Figure 2. The presence of a nanosize alloy is evident through a ring pattern. However, Pt−Au (1:1) alloy shows a broken ring due to agglomerated Pt−Au alloy particles. The XRD data shown in Figure 1 are in good agreement with electron diffraction patterns. Quantitative analyses of platinum−gold atomic ratio are performed by ICP-OES (Table 1) which indicate the bulk composition of the as-prepared Pt−Au alloy catalyst to be near the nominal value.

The surface atomic compositions for the Pt−Au alloy catalysts were also evaluated by EDAX analysis by focusing electron beam on several different selected regions. EDAX spectra for as-prepared Pt−Au alloy catalyst with varying Pt to Au atomic ratios, namely 1:1, 2:1, and 3:1, have been obtained, and it is found that the composition at various points on the surface of the samples are close to the nominal values. The EDAX compositions obtained for all the alloy catalysts prepared during this study are presented in Table 1. The data suggest that, similar to ICP-OES, the surface compositions of the as-prepared Pt−Au alloy catalysts are nearly similar to that in the bulk.

XPS for Pt (4f) core level region in Pt/C and Pt−Au/C catalysts are presented in Figure 3. Pt (4f) regions for both Pt/C and Pt−Au/C can be fitted into two sets of spin−orbit doublets. For Pt/C sample, the Pt ($4f_{7/2,\ 5/2}$) peaks at 71.13, 74.43 eV, and 72.45, 75.75 eV have been assigned to $Pt^0$ and $Pt^{2+}$, respectively. The Pt ($4f_{7/2,\ 5/2}$) doublets in (2:1) Pt−Au/C sample at 71.05, 74.35 eV and 72.37, 75.67 eV have been assigned to $Pt^0$ and $Pt^{2+}$, respectively. The relative intensities of the different species obtained from the respective peak areas are shown in Table 2. $Pt^0$ is found to be the predominant species in both Pt/C and Pt−Au/C catalysts. $Pt^0$ percentage in Pt−Au/C is 77%, which is close to 76% observed for Pt/C.

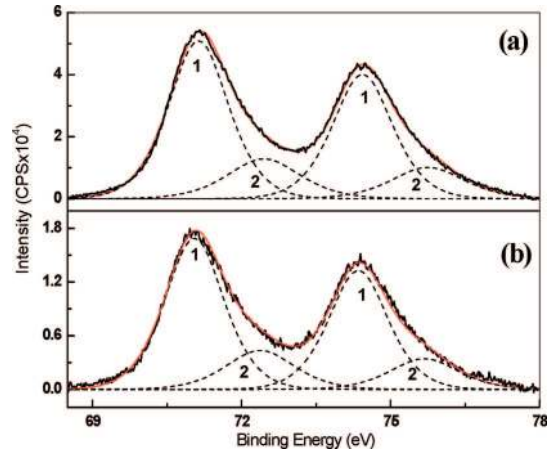


**Figure 3.** X-ray photoelectron spectra for Pt (4f) region in (a) Pt/C and (b) (2:1) Pt−Au/C catalysts. The solid line represents the fitted spectra; 1, 2 correspond to $Pt^0$ and $Pt^{2+}$ species, respectively.

**TABLE 2: Binding Energy (BE) and Relative Intensity Values for Different Pt Species As Observed from Pt (4f) XPS Spectra for Pt/C and Pt−Au/C**

| | | BE (eV) | | |
|---|---|---|---|---|
| catalyst | Pt species | $4f_{7/2}$ | $4f_{5/2}$ | relative intensity (%) |
| Pt/C | $Pt^0$ | 71.13 | 74.43 | 76 |
| | $Pt^{2+}$ | 72.45 | 75.75 | 24 |
| Pt−Au/C | $Pt^0$ | 71.05 | 74.35 | 77 |
| | $Pt^{2+}$ | 72.37 | 75.67 | 23 |

Figure 4a shows XPS for Au (4f) core level region for (2:1) Pt−Au/C catalyst. Au (4f) regions for Pt−Au/C can be fitted into two sets of spin−orbit doublets. Intense Au $4f_{7/2}$ and Au $4f_{5/2}$ lines appear at 83.50 and 87.30 eV, respectively, with a

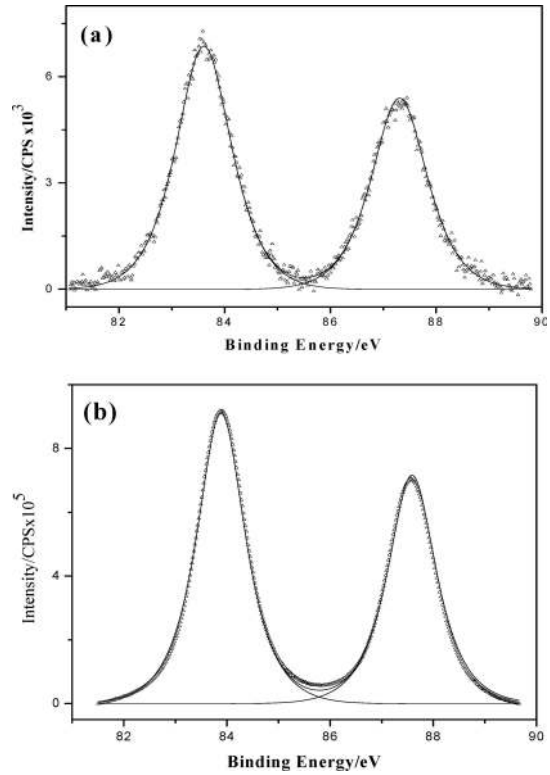


**Figure 4.** X-ray photoelectron spectra for Au (4f) region in (a) (2:1) Pt−Au/C and (b) Au foil. The solid line represents the fitted spectra.

**TABLE 3: Binding Energy (BE), fwhm, and Relative Intensity Values for Different Au Species As Observed from Au (4f) XPS Spectra for Pt−Au/C and Au Foil**

| | | BE (eV) | | |
|---|---|---|---|---|
| catalyst | Au species | $4f_{7/2}$ | $4f_{5/2}$ | fwhm (eV) |
| Pt−Au/C | $Au^0$ | 83.5 | 87.3 | 1.24 |
| Au foil | $Au^0$ | 83.88 | 87.58 | 1.33 |

theoretical ratio of 4: 3, indicating Au to be present only in metallic state in the alloy without any surface oxide. The spectral parameters obtained from the analysis of the Au ($4f_{7/2, 5/2}$) region are listed in Table 3. Figure 4b shows the XPS of Au foil (Alfa Aesar), and their spectral parameters are also presented in Table 3. The Au $4f_{7/2}$ and Au $4f_{5/2}$ lines appear at 83.88 and 87.58 eV, respectively. It is known that the presence of Au in Pt affects charge transfer from Pt to Au because of the higher electronegativity of Au (2.54) in relation to Pt (2.2).[47−49] The Au $4f_{7/2}$ binding energy obtained from the XPS (83.88 eV for Au foil and 83.50 eV for Pt−Au catalyst) supports this argument. The reduction in binding energy and full width at half maximum (fwhm) values for Au in Pt−Au alloy which is attributed to the higher electronegativity of gold in relation to Pt results in the increase of d-orbital vacancies in Pt metal.

**3.2. Electrochemical Characterization of Catalysts.** These measurements are performed to evaluate the electrochemical activity of the catalysts. Steady-state cyclic voltammograms for Pt/C and bimetallic Pt−Au/C samples in deaerated 0.5 M aq$H_2SO_4$ are presented in Figure 5. All samples exhibit the features of the hydrogen adsorption−desorption region between −0.24V and 0.1V (vs SCE) followed by the "double-layer" potential region. At potentials >0.45 V (vs SCE), oxide formation peak is observed. The hydrogen adsorption/desorption charge for the Pt−Au/C samples are smaller than the Pt/C sample. The electrochemical surface area (ECSA) derived from area under the desorption peaks are 47.2, 41.2, 32.4 and 29.8 $m^2/g$ for Pt/C, (3:1) Pt−Au/C, (2:1) Pt−Au/C, and (1:1) Pt−Au/C, respectively. A lower value of ECSA for Pt−Au catalyst is attributed to larger particle size for Pt−Au/C than Pt/C.

Methanol oxidation activity for Pt/C and Pt−Au/C with all three compositions, namely (3:1), (2:1), and (1:1), is investigated by CV in deaerated 0.5 M aq $H_2SO_4$ + 0.5 M aq $CH_3OH$ solution, and the data are presented in Figure 6. For comparison, the cyclic voltammogram of glassy carbon electrode (substrate electrode) is also included. From Figure 6, it is seen that the

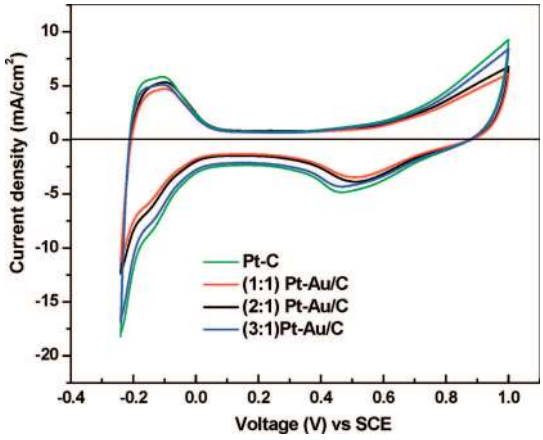


**Figure 5.** Steady-state cyclic voltammograms for the Pt/C and bimetallic Pt−Au/C catalyst with varying atomic ratios in $N_2$-saturated aq 0.5 M $H_2SO_4$ with scan rate of 50 mV/s.

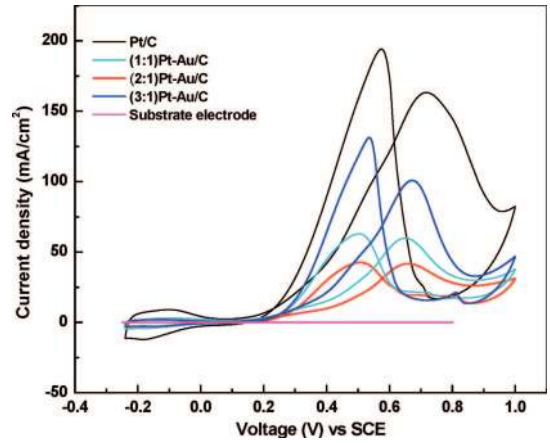


**Figure 6.** Cyclic voltammograms for Pt/C and bimetallic Pt−Au/C catalyst with various atomic ratios in $N_2$-saturated aq 0.5 M $H_2SO_4$ + aq 0.5 M $CH_3OH$ solution with scan rate 50 mV/s.

background current due to the substrate electrode is small and no peak for methanol oxidation is observed. This behavior indicates that the substrate electrode has no catalytic activity toward methanol oxidation. However, Pt/C, (3:1) Pt−Au/C, (2:1) Pt−Au/C, and (1:1) Pt−Au/C catalysts deposited on glassy carbon electrode show two oxidation peaks at 0.72 V and 0.58 V, 0.68 V and 0.53 V, 0.66 V and 0.51 V, and 0.65 V and 0.50 V, respectively, corresponding to the methanol oxidation and their intermediates produced during the methanol oxidation.[32] The magnitude of the anode peak current represents the electrocatalytic activity toward methanol oxidation.

Methanol-oxidation activity for Pt/C catalyst is higher than all Pt−Au/C catalysts. Among the Pt−Au/C catalysts, (2:1) Pt−Au/C and (1:1) Pt−Au/C exhibit lower methanol-oxidation current. It is known that the methanol adsorption−dehydrogenation process requires at least three neighboring Pt atoms with appropriate crystallographic arrangement.[31] In the Pt−Au/C samples, the probability of finding three neighboring Pt atoms on the surface decreases with increasing Au content in the alloy. Accordingly, the methanol oxidation current is smaller for (2:1) Pt−Au/C and (1:1) Pt−Au/C catalysts. In the Pt−Au alloy, Au seemingly affects the adsorption of methanol on Pt particles through platinum dilution in addition to the electronic effects. The electrocatalytic activity of gold nanoparticles toward CO and methanol oxidation reactions has been explored recently, and enhanced activity for methanol oxidation reaction on Pt−Au/C catalysts has been reported.[50,51] But these studies employ an alkaline medium where Au is known to be active for methanol oxidation. Since most of the PEM-based fuel cells employ an acidic medium, it is important to compare their behavior in acidic medium. Recently, some studies describing an enhancement of the methanol oxidation reaction in the presence of Au have been reported wherein Au is not in the form of an alloy.[52,53]

To evaluate the electrocatalytic activity of Pt/C and Pt−Au/C catalysts, LSV experiments are performed using RDE to determine the ORR with and without methanol. The LSV data are recorded in the cathodic sweep direction at 1 mV/s from 0.8 to −0.2 V vs SCE at room temperature (~25 °C). The performance of (2:1) Pt−Au/C and Pt/C catalysts toward ORR in presence and absence of methanol is shown in Figure 7. Pt−Au /C (2:1) shows higher ORR activity with least methanol-oxidation activity as shown in inset to Figure 7. The comparative data for ORR on (2:1) Pt−Au/C and Pt/C in presence and absence of methanol are also presented in Figure 7. These

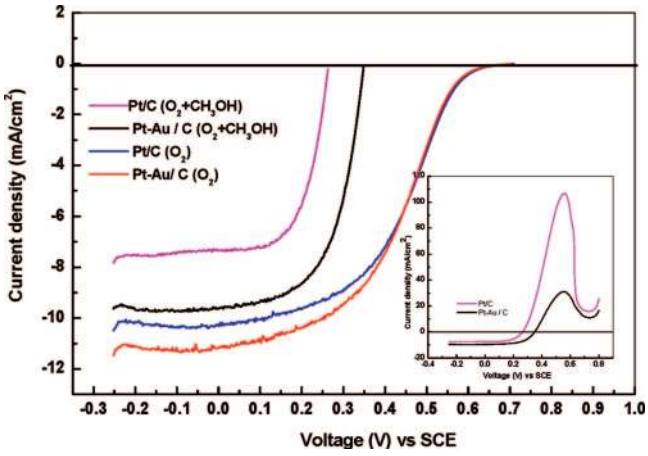


**Figure 7.** Linear sweep voltammetry (LSV) data for ORR on Pt/C and (2:1) Pt−Au/C catalysts in $O_2$-saturated aq 0.5 M $H_2SO_4$ in the presence and absence of methanol at 1 mV/s scan rate (electrode rotation rate: 1500 rpm). The inset shows the LSV data for ORR on Pt/C and (2:1) Pt−Au/C catalyst in $O_2$-saturated aq 0.5 M $H_2SO_4$ + 0.5 M $CH_3OH$.

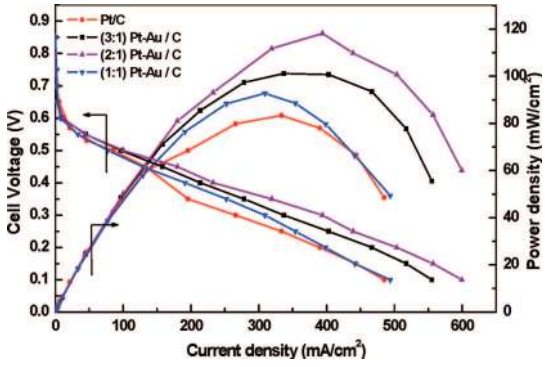


**Figure 8.** Steady-state performances of DMFCs ($CH_3OH$ and $O_2$) for Pt/C and Pt−Au/C with varying atomic ratios.

studies suggest that Pt−Au alloy shows high ORR with better methanol tolerance in relation to bare Pt catalyst. Generally, the rate-determining step for ORR is the breaking of O−O bond to form water. The kinetics of the reaction depends on the degree of interaction of oxygen with catalyst adsorption sites. The enhanced electrocatalytic activity and methanol tolerance for Pt−Au/C alloy can be explained by the electronic factor, namely, the change of the d-band vacancy in Pt upon alloying and/or by a geometric effect. Both the effects may enhance the reaction rate for oxygen adsorption and cleavage of O−O bond during the reduction reaction.

**3.3. Fuel Cell Performance.** The catalysts have also been performance tested in the DMFCs. The cell polarization data for Pt−Au/C catalysts with varying Pt to Au atomic ratios in a methanol/$O_2$ DMFC are compared with the DMFC employing Pt/C electrodes in Figure 8. It is seen that DMFC employing Pt−Au/C electrodes performs better in relation to the DMFC with Pt/C electrodes. DMFC comprising (2:1) Pt−Au/C as the cathode catalyst shows enhanced peak power density of 120 mW/cm$^2$ in relation to the peak power density of 80 mW/cm$^2$ observed for the DMFC employing Pt/C cathode. Since the anode in both the DMFCs is identical, the enhanced performance for the DMFC with Pt−Au/C catalyst is clearly due to the synergistic promotion of ORR on the catalyst. These data corroborate the CV and LSV results discussed in section 3.2.

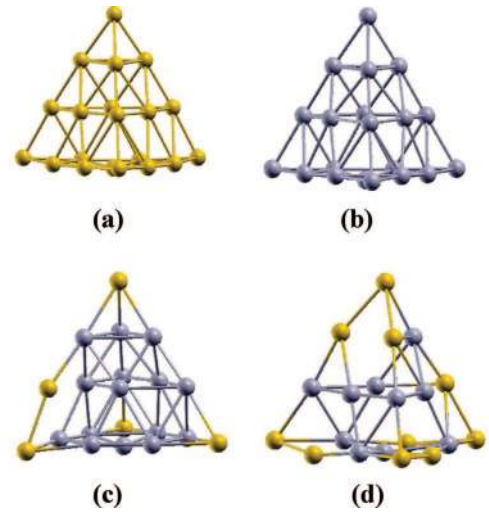


**Figure 9.** Lowest energy geometry for (a) $Pt_{20}$, (b) $Au_{20}$, (c) $Pt_{15}Au_5$, and (d) $Pt_{10}Au_{10}$.

**3.4. Catalyst Evaluation by DFT.** To further understand the higher catalytic activity at the microscopic level, the Pt−Au alloy clusters are compared with a pure Pt cluster, and resulting electronic parameters are extracted from DFT calculations. Through out this study, 20 atom clusters are used to attain the size of modeled cluster near to experimentally feasible ranges. The lowest energy configurations in fcc geometry of $Au_{20}$ and $Pt_{20}$ are shown in Figure 9a and 9b, respectively. In the case of the Pt−Au alloy cluster, the two compositions, namely $Pt_{10}Au_{10}$ (1:1) and $Pt_{15}Au_5$ (3:1), and their most stable geometries (fcc), are presented in Figure 9c and 9d, respectively. In both of these compositions, the fcc geometry is slightly distorted with Au atoms tending to occupy the corner positions (surface sites). The orientation of Au atom at surface sites is attributed to (a) the relative cohesive metal energies, (b) electronegativities, and (c) electronic/steric effects. Generally, cohesive energy ($E_{cohesive}$) of a metal, i.e., the energy required to remove an atom from the solid-state bulk metal to the gas phase, reflects the bonding energy of metal−metal interactions. $E_{cohesive}$ of 565 kJ/mol for platinum is much larger than its value of 368 kJ/mol for gold, implying that platinum atoms occupy interior sites having maximum coordination with the other metal atoms. The relative electronegativity values for Pt and Au are 2.2 and 2.54, respectively. Owing to the higher electronegativity value of Au, there is a partial charge-transfer from Pt to Au resulting in enrichment of electron density on Au surface. Accordingly, the Au atom may preferentially orient toward surface sites.

The electronic properties of bare Pt, Au, and Pt−Au alloy clusters are derived from DFT calculations, and results are

**TABLE 4: Electronic Properties of Pt, Au, and Pt−Au Clusters**

| cluster | HOMO−LUMO energy gap (eV) | Au−Pt bond distance (Å) | Pt−Pt bond distance (Å) | Au−Au bond distance (Å) | average charge on Pt (Mulliken) |
|---|---|---|---|---|---|
| $Pt_{20}$ | 0.10 | − | 2.59 | − | 0.00 |
| $Au_{20}$ | 1.79 | − | − | 2.81 | − |
| $Pt_{15}Au_5$ | 0.22 | 2.84 | 2.64 | 2.85 | 0.15 |
| $Pt_{10}Au_{10}$ | 0.31 | 2.76 | 2.68 | 2.86 | 0.23 |

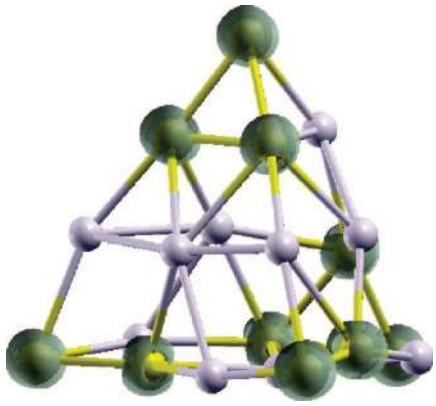

**Figure 10.** Difference charge density at 1/3 isosurface for $Pt_{10}$ $Au_{10}$.

presented in Table 4. It is known that the energy gaps between HOMO and LUMO are related to stability of the cluster.[55,56] The stability of the Pt−Au cluster increases substantially upon alloying Au with Pt. This may be responsible for the increased durability of Pt−Au alloy in relation to Pt in fuel cells.[33] There is only a small change in the Au−Au distance between the alloy and pure Au clusters. The Pt−Pt distance increases from pure to alloy clusters because of the averaging effects of alloying. In the cluster, Au−Pt distance is between Pt−Pt and Au−Au distances.

To analyze the electron redistribution in Pt−Au clusters, the difference in charge densities at one-third of their maximum are plotted as shown in Figure 10. The data suggest a charge transfer from Pt atoms to Au atoms in the alloy cluster. The absolute charge on Pt atoms for various Pt−Au alloy compositions and a homogeneous Pt cluster is estimated quantitatively, and the results are presented in Table 4. It is surmised that the high electronegativity of Au atom in Pt−Au alloy reduces the electron density on Pt atoms. It is noteworthy that, although these calculations have been carried out on small clusters with all the atoms exposed on the surface, the findings are akin to those reported in literature.[56−58] To substantiate this point, a calculation on a 36-atom Pt cluster with a single Au atom substituted at several positions was carried out. The results confirm that even in the case of clusters with a surface to volume ratio of 78%, the Au atom locates preferentially on the cluster surface with a stabilizing energy of 4.8 kcal/mol; the charge on adjacent Pt atoms in this case is 0.07. Accordingly, the electronic properties of the cluster are consistent with respect to the model and cluster size, and a charge transfer from Pt to Au atoms is confirmed. These results are in conformity with the XPS data. The positive electronic charge on Pt increases with increasing Au atomic ratios, and, accordingly, $Pt_{10}Au_{10}$ (1:1) will expectedly be a better electrocatalyst for ORR. However, as shown in Figure 8, $Pt_{10}Au_{10}$ exhibits lower activity than $Pt_{15}Au_5$ (3:1) that may be due to a high quantity of Au atoms preferentially occupying surface (corner) sites. Consequently, the access of oxygen molecules to the inner core Pt is difficult. Additionally, the higher surface availability for Au atoms in Pt−Au (1:1) may lead to agglomeration with neighboring nanoclusters. These findings are in agreement with TEM and XRD results. It is expected that the electronic parameters, such as HOMO−LUMO energy gap, atomic bond distance and average charge density for the Pt−Au cluster with an atomic ratio of 2:1 lie between $Pt_{10}Au_{10}$ and $Pt_{15}Au_5$ clusters. Our DFT calculations reflect that, in DMFCs containing Pt−Au/C in 2:1 and 1:1 ratios, the probability of finding three neighboring Pt atoms on the surface is lower than in Pt and Pt−Au (3:1), making the former more methanol tolerant in accordance with the experimental data shown in Figure 6. Accordingly, akin to our experimental findings, DFT calculations also suggest that the (2:1) Pt−Au catalyst is a better methanol-tolerant oxygen-reduction catalyst.

## 4. Conclusions

It is conjectured that (i) the mean particle size for the Pt−Au alloy catalyst increases with increasing Au content, (ii) there is a distinct intra-alloy electron transfer from Pt to Au in the Pt−Au alloy, (iii) ECSA area is maximum for Pt/C and minimum for (1:1) Pt−Au/C, (iv) linear sweep voltametry experiments suggest clear methanol-tolerant behavior for the Pt−Au catalyst toward ORR in relation to Pt, and (v) the performance of DMFC employing a (2:1) Pt−Au/C cathode catalyst is superior to the DMFC employing a Pt cathode. DFT calculations on a model cluster also reflect electron transfer from Pt to Au within the Pt−Au alloy to be responsible for the synergistic promotion of the oxygen-reduction reaction on the Pt−Au electrode.

**Acknowledgment.** Financial support from CSIR, New Delhi, through a suprainstitutional project during the EFYP is gratefully acknowledged. G. Selvarani is grateful to CSIR, New Delhi, for a Senior Research Fellowship.

## References and Notes

(1) Larmine, J.; Dicks, A. *Fuel Cell Systems Explained*, 2nd ed.; John Wiley & Sons Ltd.: England, 2003.
(2) Scott, K.; Shukla, A. K. *Modern Aspects Electrochem.* **2007**, *40*, 127.
(3) Rice, C.; Ha, S.; Masel, R. I.; Waszczuk, P.; Wieckowski, A. Tom Barnard. *J. Power Sources* **2002**, *111*, 83.
(4) Wang, J.; Wasmus, S.; Savinell, R. F. *J. Electrochem. Soc.* **1995**, *142*, 4218.
(5) Müller, J. T.; Urban, P. M.; Hölderich, W. F.; Colbow, K. M.; Zhang, J.; Wilkinson, D. P. *J. Electrochem. Soc.* **2000**, *147*, 4058.
(6) Rousseau, S.; Coutanceau, C.; Lamy, C.; Lèger, J.-M. *J. Power Sources* **2006**, *158*, 18.
(7) Shukla, A. K.; Aricò, A. S.; Antonucci, V. *Renew. Sustain. Energy Rev.* **2001**, *5*, 137.
(8) Lamy, C.; Léger, J.-M.; Srinivasan, S. In *Modern Aspects of Electrochemistry*; Bockris, J. O.' M.; Conway B. E.; White, R. E.; Eds. Kluwer Academic/Plenum Publishers: New York, 2001; 34, 53.
(9) Aricò, A. S.; Srinivasan, S.; Antonucci, V. *Fuel Cells* **2001**, *1*, 133.
(10) Liu, F.; Wang, C.-Y. *J. Electrochem. Soc.* **2007**, *154*, B514.
(11) Shukla, A. K.; Raman, R. K.; Choudhury, N. A.; Priolkar, K. R.; Sarode, P. R.; Emura, S.; Kumashiro, R. *J. Electroanal. Chem.* **2004**, *563*, 181.
(12) Hallinan, D. T.; Elabd, Y. A. *J. Phys. Chem. B* **2007**, *111*, 13221.
(13) Shukla, A. K.; Raman, R. K. *Annu. Rev. Mater. Res.* **2003**, *33*, 155.
(14) Antolini, E.; Salgado, J. R. C.; Gonzalez, E. R. *J. Electroanal. Chem.* **2005**, *580*, 145.
(15) Lima, F. H. B.; Lizcano-Valbuena, W. H.; Teixeira-Neto, E.; Nart, F. C.; Gonzalez, E. R.; Ticianelli, E. A. *Electrochim. Acta* **2006**, *52*, 385.
(16) Yuan, W.; Scott, K.; Cheng, H. *J. Power Sources* **2006**, *163*, 323.
(17) Gong, Y.; Yeboah, Y. D.; Lvov, S. N.; Balashov, V.; Wang, Z. *J. Electrochem. Soc.* **2007**, *154*, B560.
(18) Antolini, E.; Salgado, J. R. C.; dos Santos, A. M.; Gonzalez, E. R. *Electrochem. Solid-State Lett.* **2005**, *8*, A226.
(19) Hernández-Fernández, P.; Rojas, S.; Ocõn, P.; Gõmez de la Fuente, J. L.; Fabián, J. S.; Sanza, J.; Peña, M. A.; Garcìa- Garcìa, F. J.; Terreros, P.; Fierro, J. L. G. *J. Phys. Chem. C* **2007**, *111*, 2913.
(20) Mathiyarasu, J.; Phani, K. L. N. *J. Electrochem. Soc.* **2007**, *154*, B1100.
(21) Li, H.; Xin, Q.; Li, W.; Zhou, Z.; Jiang, L.; Yang, S.; Sun, G. *Chem. Commun.* **2004**, *25*, 2776.
(22) Shao, M. H.; Huang, T.; Liu, P.; Zhang, J.; Sasaki, K.; Vukmirovic, M. B.; Adzic, R. R. *Langmuir* **2006**, *22*, 10409.
(23) Haruta, M. *Nature* **2005**, *437*, 1098.
(24) Haruta, M. *Catal. Today* **1997**, *36*, 153.
(25) El-Deab, M. S.; Ohsaka, T. *Electrochem. Commun.* **2002**, *4*, 288.
(26) El-Deab, M. S.; Ohsaka, T. *J.Electranal. Chem.* **2003**, *553*, 107.
(27) Pedersen, M. O.; Helveg, S.; Ruban, A.; Stensgaard, I.; Laegsgaard, E.; Nørskov, J. K.; Besenbacher, F. *Surf. Sci.* **1996**, *426*, 395.
(28) Moller, H.; Pistorius, P. C. *J. Elecroanal. Chem.* **2004**, *570*, 243.

(29) Tekaia-Elhsissen, K.; Bonet, F.; Silvert, P. Y.; Herrera-Urbina, R. *J. Alloys Compd.* **1999**, *292*, 96.
(30) Luo, J.; Njoki, P. N.; Lin, Y.; Wang, L.; Zhong, C. J. *Electrochem. Commun.* **2006**, *8*, 581.
(31) Hernández-Fernández, P.; Rojas, S.; Ocŏn, P.; de Frutos, A.; Figueroa, J. M.; Terreros, P.; Peña, M. A.; Fierro, J. L. G. *J. Power Sources* **2008**, *177*, 9.
(32) Wang, J.; Yin, G.; Wang, G.; Wang, Z.; Gao, Y. *Electrochem. Commun.* **2008**, *10*, 831.
(33) Zhang, J.; Sasaki, K.; Sutter, E.; Adzic, R. R. *Science* **2007**, *315*, 220.
(34) Mihut, C.; Descrome, C.; Duprez, D.; Amiridis, M. D. *J. Catal.* **2002**, *212*, 125.
(35) Shimodaira, Y.; Tanaka, T.; Miura, T.; Kudo, A.; Kobayashi, H. *J. Phys. Chem. C* **2007**, *111*, 272.
(36) Song, C.; Ge, Q.; Wang, L. *J. Phys. Chem. B* **2005**, *109*, 22341.
(37) Tian, W. Q.; Ge, M.; Gu, F.; Yamada, T.; Aoki, Y. *J. Phys. Chem. A* **2006**, *110*, 6285.
(38) Ravikumar, M. K.; Shukla, A. K. *J. Electrochem. Soc.* **1996**, *143*, 2601.
(39) Selvarani, G.; Sahu, A. K.; Kiruthika, G. V. M.; Sridhar, P.; Pitchumani, S.; Shukla, A. K. *J. Electrochem. Soc.* **2009**, *156*, B118.
(40) Kresse, G.; Hafner, J. *J. Phys.: Condens. Matter* **1994**, *6*, 8245.
(41) Kresse, G.; FurthMuller, J. *Phys. Rev. B.* **1996**, *54*, 11169.
(42) Blochl, P. E. *Phys. Rev. B* **1994**, *50*, 17953.
(43) Kresse, G.; Joubert, J. *J. Phys. Rev. B* **1999**, *59*, 1758.
(44) Perdew, J. P.; Chevary, J. A.; Vosko, S. H.; Jackson, K. A.; Pederson, M. R.; Singh, D. J.; Fiolhais, C. *Phys. Rev. B* **1992**, *46*, 6671.
(45) Pykko, P. *Angew. Chem., Int. Ed.* **2004**, *43*, 4412.
(46) Li, J.; Zhai, H. J.; Wang, L. S. *Science* **2003**, *299*, 864.
(47) Goodenough, J. B.; Manoharan, R.; Shukla, A. K.; Ramesh, K. V. *Chem. Mater.* **1989**, *1*, 391.
(48) Shukla, A. K.; Aricò, A. S.; El-Khatib, K. M.; Kim, H.; Antonucci, P. L.; Antonucci, V. *Appl. Surf. Sci.* **1999**, *137*, 20.
(49) Trasatti, S. *J. Electroanal. Chem.* **1971**, *33*, 351.
(50) Zhong, C. J.; Maye, M. M. *Adv. Mater.* **2001**, *13*, 1507.
(51) Luo, L.; Maye, M. M.; Kariuki, N. N.; Wang, L.; Njoki, P.; Lin, Y.; Schadt, M.; Naslund, H. R.; Zhong, C. J. *Catal. Today* **2005**, *99*, 291.
(52) Miyazaki, K.; Matsuoka, K.; Iriyama, Y.; Abe, T.; Ogumi, Z. *J. Electrochem. Soc.* **2005**, *152*, A1870.
(53) Zhao, D.; Xu, B. Q. *Angew. Chem., Int. Ed.* **2006**, *45*, 4955.
(54) Degrand, C. *J. Electroanal. Chem.* **1984**, *169*, 259.
(55) Pearson, R. G. *Proc. Natl. Acad. Sci. U.S.A.* **1986**, *83*, 8440.
(56) Ivanov, S. A.; de Silva, N.; Kozee, M. A.; Nichiporuk, R. V.; Dahl, L. F. *J. Cluster Sci.* **2004**, *15*, 233.
(57) Grubel, G.; Gibbs, D. M.; Zehner, M.; Abernathy, D. L.; Sandy, A. R.; Mochrie, A. G. J. *Surf. Sci.* **1993**, *287*, 842.
(58) Abrams, B. L.; Vesborh, P. C. K.; Bonde, J. L.; Jaramillo, T. F.; Chorkendorff, I. *J. Electrochem. Soc.* **2009**, *156*, B273.

JP810970D